

reference potential as well as slight decomposition (as indicated by a small amount of black precipitate collecting on the electrodes, after several hours). The ~2-min rise and decay times of the IR absorption are due to cell geometry and the slow mobility of the nanocrystals. Larger nanocrystals exhibit slower time constants.

Applying a potential to a solution of CdSe nanocrystals also induces quenching of the band-edge photoluminescence. Whether delocalized in a quantum-confined state or localized in a surface state, charges can cause marked quenching of the photoluminescence in semiconductor nanocrystals (16). The same effect is observed in the electrochemical electron injection. The “on/off” behavior of the photoluminescence properties of CdSe/ZnS core/shell nanocrystals is seen (Fig. 4A) as the electrochemical potential is varied (set at either 0 or -1.5 V). The photoluminescence spectra of CdSe/ZnS (Fig. 4B) correspond to points (i), (ii), and (iii) in Fig. 4A. The photographs of the sample under UV illumination (Fig. 4C) show that photoluminescence quenching is readily observed by eye and occurs mostly near the working-electrode disk. The spatial selectivity of photoluminescence quenching may be desirable in display applications.

At -1.5 V, the photoluminescence quenches to ~40% of the initial value in 1 min and recovers completely in ~60 min after the potential is reset to 0 V. The slower photoluminescence recovery rate with respect to the IR absorption decay may be attributed to the effects of surface charges; that is, the IR absorption depends only on the electrons in the 1S state, whereas the photoluminescence can be strongly quenched by charges in the surface band-gap states. For the photoluminescence to recover to its maximum, electrons in both the 1S state and surface states need to be removed. Improvements in surface passivation, experimenting with different electrolytes and different materials, and investigating thin solid-film electrodes are likely to lead to technologically practical and efficient electrochemical switching of the optical properties of colloidal nanocrystal quantum dots.

References and Notes

1. M. Nirmal, L. E. Brus, *Acc. Chem. Res.* **32**, 407 (1999).
2. A. P. Alivisatos, *Science* **271**, 933 (1996).
3. C. B. Murray, C. R. Kagan, M. G. Bawendi, *Science* **270**, 1335 (1995).
4. M. A. Kastner, *Phys. Today*, 24 (1993).
5. R. C. Ashoori, *Nature* **379**, 413 (1996).
6. V. Colvin, M. Schlamp, A. P. Alivisatos, *Nature* **370**, 354 (1994).
7. B. O. Dabbousi, M. G. Bawendi, O. Onitsuka, M. F. Rubner, *Appl. Phys. Lett.* **66**, 1316 (1995).
8. B. O'Regan, M. Grätzel, *Nature* **353**, 737 (1991).
9. T. Yamase, *Chem. Rev.* **98**, 307 (1998).
10. C. G. Granqvist, *Sol. Energ. Mat. Sol. Cells* **60**, 201 (2000).

11. U. zum Felde, M. Haase, H. Weller, *J. Phys. Chem. B* **104**, 9388 (2000).
12. C. B. Murray, D. J. Norris, M. G. Bawendi, *J. Am. Chem. Soc.* **115**, 8706 (1993).
13. M. A. Hines, P. Guyot-Sionnest, *J. Phys. Chem. B* **102**, 3655 (1998).
14. O. I. Micic *et al.*, *J. Phys. Chem.* **98**, 4966 (1994).
15. M. Shim, P. Guyot-Sionnest, *Nature* **407**, 981 (2000).
16. M. Shim, C. Wang, P. Guyot-Sionnest, *J. Phys. Chem. B*, in press.
17. P. Hoyer, H. Weller, *Chem. Phys. Lett.* **221**, 379 (1994).
18. M. A. Hines, P. Guyot-Sionnest, *J. Phys. Chem.* **100**, 468 (1996).
19. R. E. Wittig, C. P. Kubiak, *J. Electroanal. Chem.* **393**, 75 (1995).
20. We have not yet observed hole injection most likely because of other oxidative processes that prevent it. Applying a positive potential (0 to +3 V) to the samples did not cause changes in the visible absorption or photoluminescence properties of the nanocrystals. Successful hole injection will require an optimization of solvent and electrolyte combination as well as nanocrystals that are stable after oxidation.

21. N. M. Dimitrijevic, D. Savic, O. I. Micic, A. J. Nozik, *J. Chem. Phys.* **88**, 4278 (1984).
22. B. Enright, G. Redmond, D. Fitzmaurice, *J. Phys. Chem.* **98**, 6195 (1994).
23. The confinement energy,  $E_x - E_g$ , can be approximated as  $\hbar^2/2m^*R^2$  and the charging energy,  $E_c$ , as  $e^2/2\epsilon R$ .  $E_x$  is the first exciton transition energy,  $E_g$  is the bulk band gap,  $R$  is the radius of the nanocrystals,  $m^*$  is the effective mass of the electron, and  $\epsilon$  is the dielectric constant of the solvent. With the bulk reduction potential,  $V_o$ , the reduction potential,  $V_r$ , of nanocrystals can be expressed as  $[(E_x - E_g) + E_c]/e + V_o$ .
24. R. Memming, *Top. Curr. Chem.* **169**, 105 (1994).
25. R. J. D. Miller, G. L. McLendon, A. J. Nozik, W. Schmickler, F. Willig, *Surface Electron Transfer Processes* (VCH, New York, 1995), p. 44.
26. Funded by a grant from the National Science Foundation (DMR-9731642). Experiments made use of the Materials Research Science and Engineering Centers Shared Facilities supported by a grant from the National Science Foundation (DMR-9400379).

28 November 2000; accepted 1 February 2001

## In Situ Measurement of Grain Rotation During Deformation of Polycrystals

L. Margulies,<sup>1,2</sup> G. Winther,<sup>1</sup> H. F. Poulsen<sup>1\*</sup>

Texture evolution governs many of the physical, chemical, and mechanical properties of polycrystalline materials, but texture models have only been tested on the macroscopic level, which makes it hard to distinguish between approaches that are conceptually very different. Here, we present a universal method for providing data on the underlying structural dynamics at the grain and subgrain level. The method is based on diffraction with focused hard x-rays. First results relate to the tensile deformation of pure aluminum. Experimental grain rotations are inconsistent with the classical Taylor and Sachs models.

Most metals and ceramics are aggregates of crystalline grains. The crystalline lattice of each grain has a characteristic orientation, and a polycrystal is thus characterized by a distribution of orientations—its texture. The texture plays a role in virtually every modern industry, determining phenomena as diverse as the weight of beer cans and the prospect of high-temperature superconducting cables. The orientation difference between neighboring grains is the focus of an emerging technology termed “grain boundary engineering.” At the same time, textures in minerals and rocks are vital sources revealing information about geological processes.

Textures evolve during plastic deformation,

where a polycrystal changes its shape. At the grain level, each grain changes its shape and its crystallographic lattice rotates. The external force produces line defects (dislocations) in the lattice. The dislocations move in certain directions (slip directions) within certain planes (slip planes), causing the two sides of the plane to slide with respect to each other. The change in grain shape is the result of millions of such operations. The dynamics of the grains are coupled, because the two sides of any grain boundary at all times must adjoin and be in stress equilibrium. To facilitate this process, the grains have to change shapes in different ways, and their crystallographic orientations must rotate with respect to each other.

Various texture models have been presented in the literature for more than 50 years. They predict which possible slip systems (combinations of slip plane and slip direction) are operational and calculate the resulting texture and other macroscopic properties,

<sup>1</sup>Materials Research Department, Risø National Laboratory, 4000 Roskilde, Denmark. <sup>2</sup>European Synchrotron Radiation Facility, BP 220, 38043 Grenoble, France.

\*To whom correspondence should be addressed. E-mail: henning.friis.poulsen@risoe.dk

## REPORTS

such as the yield stress. However, many central issues remain unsolved, because the grain dynamics have not been observed directly. In particular, conventional techniques, such as optical and electron microscopy as well as laboratory-based x-ray diffraction, probe the near surface. The free surface leads to stress relaxation, which makes dynamic studies using these techniques irrelevant. Hence, experimental verification is only possible by averaging over grains, typically by a statistical analysis.

Because of the lack of local-scale experimental input, models are based on global assumptions without taking the different surroundings of individual grains into account. These assumptions deal with the ambiguity in choosing between a number of possible operational slip systems, which have nearly the same energy, and the issue of which strain and stress conditions to impose on the grain boundaries. The classical models are the Taylor model (1), which assumes that all of the grains are subject to the same strain, and the Sachs model (2), which assumes only the most stressed slip system to be operational. Self-consistent models that consider the interaction between a grain and a surrounding matrix representing the average bulk behavior are also used (3). In general, these models and refinements thereof (4) exhibit mathematical singularities and differ substantially. For example, the predicted number of operational slip systems varies between 1 and 8.

Despite the huge modeling effort, present models cannot account for texture evolution; most noteworthy is the general overestimation of the rate of texture development (4). Another feature not grasped by any of the models is that, during deformation, grains break up on a micrometer scale into fairly regular deformation structures with different crystallographic orientations (5). To facilitate the establishment of models taking such fea-

tures into account, one needs local-scale dynamic data.

Here, we present results on the rotation and subdivision of bulk grains during deformation. Such studies have been attempted twice before with split samples (6, 7). In both cases, the internal surfaces of split samples were investigated, then fitted together. After deformation, the samples were disassembled and the internal surfaces were reinvestigated. The results are questionable, because the effect of the interface is unknown and the experiment only allows two-dimensional characterization of the grain surroundings. In contrast, our method of choice investigates a grain while it is deeply embedded in a polycrystal. Furthermore, the method can be extended to provide a characterization in three dimensions.

The method is three-dimensional (3D) x-ray diffraction microscopy, recently developed and put into use at the European Synchrotron Radiation Facility (8-11). The experimental setup is shown in Fig. 1. The tensile specimen is high-purity aluminum (99.996%) with a thickness of  $t = 3$  mm and an average grain size of  $300 \mu\text{m}$ . It is mounted in a stress rig, which is fixed to a sample stage, that allows  $x$ ,  $y$ , and  $z$  translations as well as a rotation of magnitude  $\omega$  about the  $z$  axis. A hard x-ray beam with an energy of 50 keV (and a penetration power of centimeters) is focused on the specimen and illuminates a volume of  $5 \mu\text{m}$  by  $300 \mu\text{m}$  by  $t$ . Some of the grains within this volume will give rise to diffracted beams (reflections) that are transmitted through the sample to appear as spots on a charge-coupled device camera. At each strain, 25 images were recorded while stepping from  $-12^\circ$  to  $12^\circ$  in  $\omega$ , around the position  $\omega = 0^\circ$ , where the tensile axis is perpendicular to the beam. All of the images were acquired in 1 s while oscillating the sample by  $1^\circ$  in  $\omega$  around its nominal value to ensure full integration of the intensity for grains with some intragranular orientation

spread. In this way, each grain gives rise to a minimum of six recorded reflections. Measurements were made for strains of 0, 2, 4, 5, 7, 9, and 11%.

Four grains positioned near the center of the specimen were identified by x-ray tracing (9, 10). At each strain level, these grains were centered in the  $y$  and  $z$  directions by examining the integrated intensity of a reflection during translation of the sample. As sketched in the enlarged part of Fig. 1, the illuminated volume contains many grains. An automatic indexing program was used to sort out the reflections from the four grains of interest from a background arising from all other grains and to calculate the orientations of the four grains (10).

Examples of raw data are shown in Fig. 2. Initially, any reflection appears as a spike in one image that corresponds to one specific  $\omega$  setting. With increasing strain, the reflection moves on the unit sphere, so that the spot appears at a different  $\omega$  setting and moves along the azimuthal direction  $\eta$  (see Fig. 1 for definition of  $\eta$ ). The spots also broaden in the two directions, which eventually leads to an overlapping of spots. With the present setting, a sufficient number of non-overlapping reflections were available at all strain levels.

**Fig. 1.** Sketch of experimental setup. Coordinate system ( $x$ ,  $y$ ,  $z$ ) and angles ( $\omega$ ,  $2\theta$ ,  $\eta$ ) are defined. All of the grains within the stripe illuminated by the beam will give rise to diffracted spots during the scanning of  $\omega$ . Spots are further characterized by their Bragg angle  $2\theta$  and their position on the Debye-Scherrer ring given by  $\eta$ .

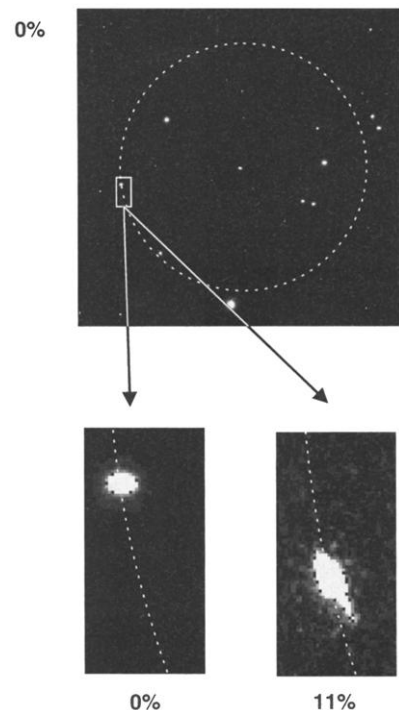
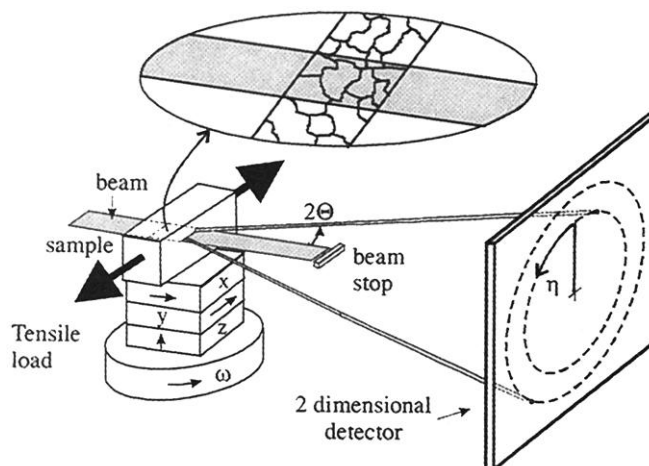


**Fig. 2.** Example of raw data for  $\omega = 1^\circ$  and 0% strain (top). The circle marks the (220) Debye-Scherrer ring, and the box identifies a spot related to grain 1. The enlarged areas (bottom) show the movement of this spot on the ring, by comparison with a corresponding image at  $\omega = -5^\circ$  and 11% strain.

The average rotation and the spread of orientations developed during deformation are illustrated in Fig. 3 for the same reflection as depicted in Fig. 2. The average rotation velocity is 5.5° per 11% deformation. The spread at a strain of 11% is ~2°, which is consistent with transmission electron microscopy measurements of typical misorientation angles across deformation-induced dislocation boundaries in the same material (12). The increase in spread is one-fourth the rotation rate. Here, a ratio of, say, 1:1 would imply a direct rejection of all present models, whereas a ratio of 1:20 or more would indicate that grain breakup can be neglected.

The rotations of the tensile axis for the four grains are presented in Fig. 4. The results are compared with predictions of the classical Taylor and Sachs models by using the antisymmetric part of the strain tensor to calculate the crystallographic grain rotations. These models are usually regarded as upper and lower bound models with respect to the applied work. (Corresponding results for the rotation of the sample normal perpendicular to the tensile axis are consistent with the conclusions below.)

For the Taylor model, all of the solutions to the ambiguity problem with the same five slip systems (or as similar as possible in the case of rotation to orientations where new slip systems are activated) are shown in Fig. 4A; that is, the model predicts any linear combination of the solutions shown. For grain 1, the model has substantial ambiguity, and thus rotation in any direction except toward the <110> corner is predicted. The experimental data fall within this large span of directions. For grain 3, the Taylor model is also associated with a large ambiguity, but the experimentally observed rotation toward the <111> corner is totally unpredicted. For grains 2 and 4, the experimental rotations clearly lie to the left of the narrow span of predicted rotation directions.

The Sachs model has no ambiguity (Fig.

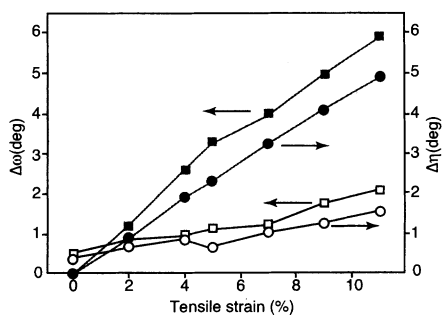


**Fig. 3.** Experimental data for the average rotation (solid symbols) of the reflection singled out in Fig. 2, compared with the spread in orientation (full width at half maximum) of the same reflection (open symbols). Shown are the components along the change in two experimental angles,  $\Delta\omega$  and  $\Delta\eta$ , defined in Fig. 1.

4B). Here, model predictions of the direction agree well with the experimental data for grain 4 but lie to the left of the experimental data for the other three grains. The correct prediction of the final orientation of grain 2 appears to be accidental because the model clearly fails in predicting the path to this orientation. We conclude that neither model works, but for three out of the four grains, the experimental rotation of the tensile axis lies between the predictions of the Taylor and Sachs models; that is, the grains move toward the predicted dominant stable orientation in the <111> corner.

The experimental rotation rates follow the Taylor model well and are lower than the predictions from the Sachs model. The reason for the difference between models is that the Taylor model operates with more slip systems (five to eight active systems) than does the Sachs model (one system) and that coactive slip systems tend to counterbalance each other. Hence, the results

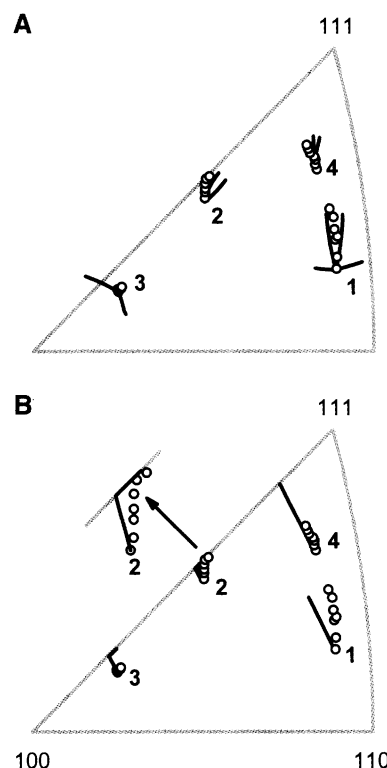


**Fig. 4.** The dynamics of four embedded aluminum grains during tensile deformation. Experimental data (open circles) are shown as inverse pole figures, which represent the position of the tensile axis in the reciprocal space of the grains. Strain levels were 0, 2, 4, 5, 7, 9, and 11%. The instrumental errors are substantially smaller than the symbol size. A comparison is performed with the evolution path from 0 to 11% (solid line) as predicted by (A) a full-constraints Taylor model and (B) a Sachs model. Several lines associated with the same grain represent degenerate solutions. To show the comparison, we enlarged the data set for grain 2.

indicate that the grains deform by multislip.

A ratio of grain size versus specimen size of 1:15 has been shown to eliminate surface effects on the mechanical properties of the whole specimen (13). It is therefore concluded that the four grains analyzed, which were situated in the center of the specimen with a 1:10 ratio, must represent the bulk. In general, limitations of specimen thickness are set by the penetration power of the hard x-rays (penetration of several millimeters is universally available and can be as much as 5 cm for aluminum). Limitations on the grain size are set by the breakup, which smears out the peaks. For the strain levels used here, a grain size of 10  $\mu\text{m}$  is realistic.

The technique presented above allows simultaneous measurements on a number of grains and enables statistical analysis for ensembles of grains. Moreover, by scanning the detector parallel to the incoming beam, a 3D grain map can be extracted (10). Hence, information on neighboring relations is available. Simultaneously, by generating 3D maps of grain boundaries before and after the deformation, the shape changes of the grains can be produced. All of the necessary information for the establishment and tests of local models, such as finite-element algorithms, is then provided. Simultaneously, the described technique bridges the grain and subgrain length scales (compare with Fig. 3). Definite answers to the question of texture evolution seem therefore finally at hand.

**References and Notes**

- G. I. Taylor, *J. Inst. Met.* **62**, 307 (1938).
- G. Sachs, *Z. Ver. Dtsch. Ing.* **72-22**, 734 (1928).
- E. Kröner, *Acta Metall.* **9**, 155 (1961); J. W. Hutchinson, *Proc. R. Soc. London Ser. A* **319**, 247 (1970).
- U. F. Kocks, C. N. Tomé, H.-R. Wenk, *Texture and Anisotropy: Preferred Orientations in Polycrystals and Their Effect on Materials Properties* (Cambridge Univ. Press, New York, 1998).
- B. Bay, N. Hansen, D. A. Hughes, D. Kuhlmann-Wilsdorf, *Acta Metall. Mater.* **40**, 205 (1992).
- C. S. Barrett, L. H. Levenson, *TMS-AIME* **137**, 112 (1940).
- S. Panchanadeeswaran, R. Becker, R. D. Doherty, K. Kunze, *Mat. Sci. Forum* **157-162**, 1277 (1994).
- H. F. Poulsen et al., *J. Synchrotron Radiat.* **4**, 147 (1997).
- D. Juul Jensen et al., *Mater. Res. Soc. Symp. Proc.* **590**, 227 (2000).
- D. Juul Jensen, H. F. Poulsen, in *Proceedings of the 21st Risø International Symposium on Materials Science, Risø 4-8 September 2000*, N. Hansen et al., Eds. (Risø National Laboratory, Roskilde, Denmark, 2000), p. 103; S. F. Nielsen et al., in *Proceedings of the 21st Risø International Symposium on Materials Science, Risø 4-8 September 2000*, N. Hansen et al., Eds. (Risø National Laboratory, Roskilde, Denmark, 2000), p. 473.
- S. F. Nielsen et al., *J. Synchrotron Radiat.* **7**, 103 (2000).
- X. Huang, personal communication.
- N. Hansen, *Acta Metall.* **25**, 863 (1977).
- This work was supported by the Danish Natural Science Research Council through Dansync. We thank N. Hansen, T. Lorentzen, R. M. Suter, U. Lienert, D. Juul Jensen, and T. Leffers for advice and help with experimental work.

1 December 2000; accepted 13 February 2001